Selective oxidation and ammoxidation of propene on bismuth molybdates, *ab initio* calculations

Yun Hee Jang * and William A. Goddard III **

Materials and Process Simulation Center (139-74), California Institute of Technology, Pasadena, CA 91125, USA
E-mail: wag@caltech.edu

In this paper we use first principles quantum mechanical methods (B3LYP flavor of density functional theory) to examine the mechanism of selective oxidation and ammoxidation of propene by $BiMoO_x$ catalysts. To do this we use finite clusters chosen to mimic likely sites on the heterogeneous surfaces of the catalysts. We conclude that activation of the propene requires a Bi(V) site while all subsequent reactions involve di-oxo Mo(VI) sites adjacent to the Bi. We find that two such Mo sites are required for the most favorable reactions. These results are compatible with current experimental data. For ammoxidation, we conclude that ammonia activation would be easier on Mo(IV) rather than on Mo(VI). Ammonia would be activated more easily for more reducing condition. Since ammonia and propene are reducing agents, higher partial pressures of them could accelerate the ammonia activation. This is consistent with the kinetic model of ammoxidation proposed by Grasselli and coworkers that imido sites (Mo=NH) are more abundant in higher partial pressures of feed. Our calculations also indicate that allyl groups produced as a result of the hydrogen abstraction from propenes would be adsorbed more easily on imido groups (Mo=NH) than on oxo groups (Mo=O) and that the spectator oxo effect is larger than spectator imido effect. Thus, we propose that the best site for ammoxidation (at least for allyl adsorption) is the imido group of the "oxo–imido" species.

KEY WORDS: selective oxidation; ammoxidation mechanism; bismuth molybdates; density functional theory; cluster model

Foreword

I am most pleased to be here in Irsee Germany to honor Bob Grasselli on his 70th birthday. I first met Bob at an Industrial Associates Conference at Stanford (it must have been ~1981), where I was talking about some recent work that Tony Rappé and I had done on metathesis of olefins by $MoCl_6$-based catalysts. Barry Sharpless, then on the Stanford faculty, had invited me (the competition for industrial interactions from Caltech) because he knew about our ideas on spectator oxo groups. My talk concluded that there must be a "spectator" oxo group in the active catalyst in addition to the alkylidene and showed that this spectator oxo group was necessary to promote the reaction at the adjacent alkylidene [1–3]. This suggestion had been subsequently confirmed experimentally. I went on to show why such spectator groups promote reactions at adjacent multiple bonds and suggested that this concept could be used to design new catalysts. Bob commented that my work was fine and interesting, but if I wanted to do something really important, I should work on ammoxidation (which at that point I had not heard of). At this conference Bob reported some of the recent work he and Jim Burrington had done on the mechanism of selective oxidation and ammoxidation. I was quite impressed by the clever approaches that Jim and Bob had used to pin down the organic species involved, but I did not believe that a single Mo could do the job. I thought that probably every important step would involve Mo=O and Mo=NH spectator groups.

Bob's work stimulated me to ask Tony Rappé to examine the role of oxo and di-oxo species in heterogeneous systems. This led to a paper on oxidations (but not ammoxidation) by Mo(VI) oxides, where we concluded that the di-oxo species would be the effective catalysts [4]. I then suggested to a new graduate student, Janet Allison, that ammoxidation would be a neat system to examine, which she proceeded to do over the next couple of years [5]. We concluded that the active sites started as Mo with two Mo=O oxo bonds; that a single Mo=O site could not do the chemistry. Thus two such sites were required to produce acrolein and four were required to form acrylonitrile. We also concluded that the oxo–imido site should be best for ammoxidation. We concluded that these sites were favored at the surfaces of the mixed oxides. I do not know whether Jim and Bob believed our results, because I do not believe that they ever modified their mechanism. However, Bob did hire me as a consultant at SOHIO, and we became good friends as we interacted on various areas of catalysis.

The discoveries made by Bob and his team at SOHIO are tremendously impressive, showing keen insight into the chemistry, a penchant for developing real mechanisms to gain increased understanding, and then using this understanding to direct experiments toward the most promising directions. This willingness to replace Edisonian strategies with mechanistically driven research is, I believe, the reason why SOHIO in the Grasselli days was so tremendously successful in developing industrial catalysts that remain important today. Although Bob's accomplishments are generally recognized in the catalysis community, it seems to me that they have never been fully appreciated in the broader chemical community (for example, Bob's accomplishments have

* Current address: School of Chemistry, Seoul National University, Seoul 151-747, Korea.
** To whom correspondence should be addressed.

1022-5528/01/0600-0273$19.50/0

not been recognized by election to the US National Academy of Sciences). Indeed his award of the Morley prize, given by the Cleveland section of the ACS did not occur until May 1999!

In addition to his ability as a scientist, Bob was a tremendous manager at SOHIO. He had the uncanny ability to immediately size up people that could think creatively and to solve problems, building a research organization at SOHIO that was truly impressive.

Bob has had impact in many other areas. One that may not be so well known is that Bob was the driving force in getting the Gordon Conference Trustees to broaden the base from the US to Europe and Asia. To do so he had to make many trips to Europe, trying out potential sites and making deals that would be attractive to the Trustees. Then he had to convince a somewhat stodgy group of Trustees that it made sense. With help from his friends Bob finally won.

In deciding what to talk about at this conference, I decided to reexamine the calculations we had done on selective oxidation and ammoxidation in the early 1980s. At the time, the methods of using *ab initio* quantum mechanics on heterogeneous (or homogeneous) catalysts were so primitive, that we had to make many short cuts and simplifications. The advances in the methods and in computers have dramatically improved our ability to do such studies with fewer simplifications, making it useful to re-examine these systems. This is also relevant to current catalyst development. Thus the advances by Mitsubishi and BP America in developing ammoxidation catalysts that operated on propane rather than propene, suggests that there are still great opportunities in designing improved catalysts for such systems.

1. Introduction

Despite the keen industrial interest in selective oxidation and ammoxidation of small alkanes (CH_4, C_2H_6, C_3H_8, and C_4H_{10}) by mixed metal oxides, there is little in the way of definitive mechanisms known for the most effective catalysts. In order to learn more about the reaction mechanism of these important catalysts, we are using a variety of first principles theoretical approaches to calculate the fundamental steps.

As the first step, we examined the selective oxidation and ammoxidation of propene [6,7] for which there are some experimental data relating to mechanism:

$$CH_3CHCH_2\ (\text{propene}) + O_2 \xrightarrow{300\text{–}450\,^\circ C} CH_2CHCHO\ (\text{acrolein}) + H_2O \quad (1)$$

$$CH_3CHCH_2\ (\text{propene}) + NH_3 + 1.5O_2 \xrightarrow{400\text{–}460\,^\circ C} CH_2CHCN\ (\text{acrylonitrile}) + 3H_2O \quad (2)$$

One of the most active and selective catalysts for these reactions is based on bismuth molybdate [7–9]. The mechanism has been proposed as (scheme 1) [10,11]:

(1) allylic H abstraction at a bismuth site resulting in the allyl intermediate adsorbing on a molybdenum site (rate-determining step),

(2) O insertion into the allyl intermediate at the molybdenum site and abstraction of a second H,

(3) elimination of the H_2O to remove the H from the bismuth oxide, and

(4) reoxidation of the Bi and Mo sites.

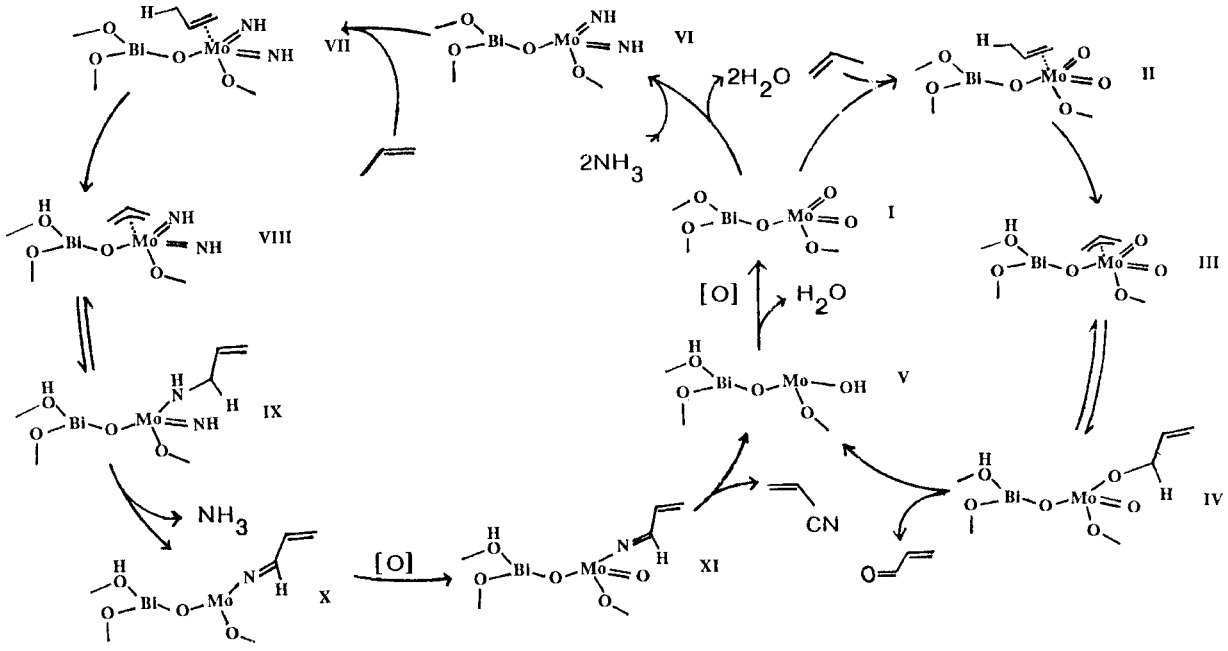

Scheme 1. Proposed mechanism. Burrington, Kartisek and Grasselli [11].

The "dual-site" concept is widely accepted, where the bismuth site is responsible for the C–H activation and the molybdenum site is responsible for allyl adsorption and oxygen insertion. Ammoxidation proceeds essentially in the same way as oxidation, except that (1) ammonia is first activated on molybdenum site to create imido groups (=NH) from oxo groups (=O) and (2) NH rather than O is inserted into allyl group.

In this study, we investigated this reaction path on the model clusters of the component oxides (Bi_2O_3 and MoO_3) using *ab initio* quantum-mechanical (QM) methods (DFT-B3LYP).

2. Calculation details

2.1. Model clusters

A schematic representation of the crystal structures of the component oxides of bismuth molybdate, α-MoO_3 and α-Bi_2O_3, is given in figure 1. In α-MoO_3 [12], each molybdenum site consists of a tetrahedron with two terminal oxo oxygens (r(Mo=O) $\approx$ 1.7 Å) and two bridging oxygens (r(Mo–O) $\approx$ 1.9 Å) connected to a molybdenum atom in its nearest-neighbor coordination shell. In α-Bi_2O_3 [13], each bismuth has three nearest-neighbor oxygens connected to it and one lone pair. Similar bonding configuration can be found in one of the bismuth molybdates, α-$Bi_2Mo_3O_{12}$ [14,15], as shown in figure 1(c).

In order to represent each site, we chose the model clusters having the same stoichiometry and connectivity as in the crystal structure. The Bi_4O_6 cluster (figure 2(a)) has three oxygens connected to each bismuth atom, and the Mo_3O_9 cluster (figure 2(b)) has two terminal oxo oxygens and two bridging oxygens connected to each molybdenum atom.

The Mo_3O_9 cluster has been found to be one of the most abundant gas-phase molybdenum oxide cluster species (cations and anions) generated from the evaporation of the MoO_3 oxide samples from an effusion source (Knudsen cell) [16–18]. Its six-ring structure has been suggested as the lowest-energy structure [16,18]. The Bi_4O_6 cluster in the adamantane-type cage structure has been proposed as a neutral species present in the gas phase [19–22], and the cationic species $Bi_4O_6^+$ has been recently detected from the laser vaporization experiment from a bismuth rod with an expansion gas seeded with oxygen [23]. There have been many recent experiments on the reaction of these mass-selected gas-phase metal oxide clusters with small molecules such as ammonia, ethene and propene as a model study of the het-

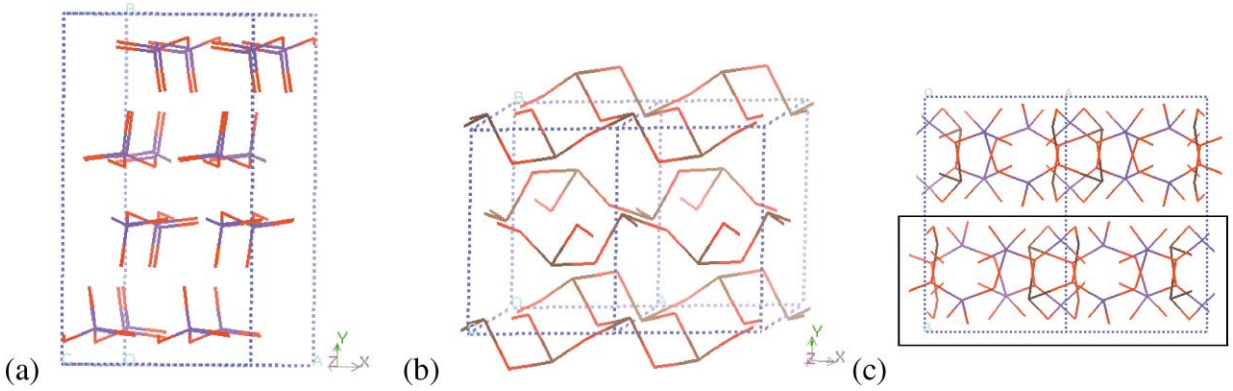

Figure 1. Crystal structures of the component oxides of bismuth molybdate. (a) α-MoO_3 [12] and (b) α-Bi_2O_3 [13]. (c) Crystal structure of one of phases bismuth molybdate, α-$Bi_2Mo_3O_{12}$ [14,15].

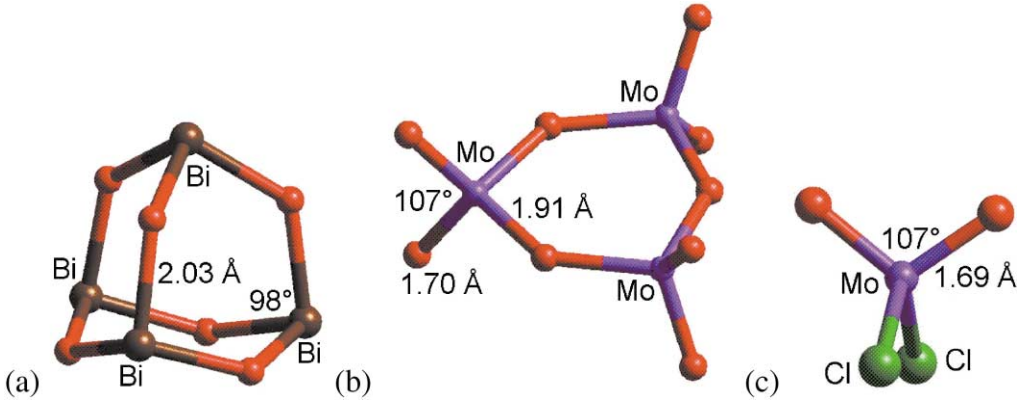

Figure 2. Model clusters used to represent (a) the bismuth site (Bi_4O_6) and (b) the molybdenum site (Mo_3O_9). (c) Smaller model cluster used to represent the molybdenum site instead of (b) in the later part of the work.

Table 1
Dissociation energies D_{298} (kcal/mol) of relevant molecules calculated at 298 K with the B3LYP flavor of restricted open-shell density-functional theory (RODFT). For comparison, the values calculated at other DFT levels (B3LYP, BLYP and PW91 flavors of unrestricted DFT) are also listed. For the unrestricted DFT calculations, Jaguar v4.0 was used.

	RODFT	UDFT			Experiment[a]	
	B3LYP	B3LYP	BLYP	PW91		
H–CH_3	104.6	103.6	102.9	103.4	104.9 ± 0.1[b]	$\Delta H(^2CH_3) + \Delta H(^2H) - \Delta H(CH_4)$
H–CH_2CHCH_2	86.8	84.4	82.9	83.7	86.5 ± 2.1[b,c]	$\Delta H(^2\text{allyl}) + \Delta H(^2H) - \Delta H(\text{propene})$
Bi–O	84.5	84.5	100.0	97.6	81 ± 3[d,e]	$\Delta H(^4Bi) + \Delta H(^3O) - \Delta H(^2BiO)$
Mo–O	113.1	113.8	133.8	131.6	134 ± 5[d], 125.4 ± 0.9[f]	$\Delta H(^7Mo) + \Delta H(^3O) - \Delta H(^5MoO)$

[a] From [36].
[b] From [37].
[c] From [38].
[d] From [39].
[e] Other experimental data: (1) 81.0 ± 1.4 kcal/mol [40]; (2) 79.6 ± 0.7 at 0 K [22]. At 0 K we calculate $D_0 = 83.71$ kcal/mol (B3LYP).
[f] From [41].

erogeneous catalysis [18,23–25]. Consequently, our calculations employing these model clusters should help interpret the experimental results.

Our studies find that the terminal oxo oxygens lead to reactions on the Mo site that are far more favorable than for the bridging oxygens (see section 3.1). Appendix compares the energetics for several key processes with the Mo_3O_9 cluster with the results on the smaller MoO_2Cl_2 (figure 2(c)) cluster in which the bridging oxygen atoms are replaced with chlorine atoms. We find essentially identical energetics. Consequently most of our studies on the mechanism used the smaller MoO_2Cl_2 cluster.

2.2. Calculational methods

2.2.1. Quantum mechanics

We used the B3LYP flavor of density-functional theory (DFT) which includes the generalized gradient approximation and a component of the exact Hartree–Fock (HF) exchange [26–30]. The Dunning cc-pVTZ(-f) basis set [31,32] was used for H, C, N, and O. The effective core potentials (ECP) and basis set of Hay and Wadt were used for Mo and Bi (LACVP**) [33]. The 6-31G** basis set was used for chlorines (Cl) replacing bridging oxygens. All the calculations were carried out using Jaguar 3.5 (except as noted) [34,35].

2.2.2. Energetics

For each structure the geometry was fully optimized and shown to be a minimum. Vibration frequencies were calculated from the Hessian (second derivative matrix) and used to obtain zero-point energies and thermodynamic properties (enthalpy and free energy) at the reaction temperature of 673 K as in (3) or at room temperature (298 K):

$$\Delta G_{673\,\mathrm{K}} = E + \mathrm{ZPE} + \Delta\Delta G_{0\to 673\,\mathrm{K}}. \qquad (3)$$

The dissociation energies (enthalpies), D_{298}, of several relevant molecules are given in table 1, indicating good agreement between calculation and experiment.

Table 2
C–H bond strengths of propene in the gas phase. (a) Bond dissociation enthalpy D_{298} (kcal/mol) at 298 K and (b) bond dissociation free energy at 673 K during C–H cleavage from C_3H_6 to $^2C_3H_5$ (three different bonds).

	(a) D_{298} at 298 K	(b) ΔG at 673 K
C_α–H_α	86.8	69.8
C_β–H_β	105.7	87.4
C_γ–H_γ	110.8	92.6

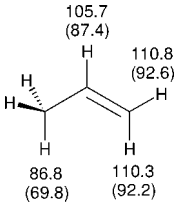

3. Oxidation

3.1. First step: H-abstraction

The calculated C–H bond strengths of propene are listed in table 2. As expected the C_α–H_α bond is weakest, leading to $D_{298} = 86.8$ kcal/mol in excellent agreement with the experimental value of 86.5 ± 2.1 kcal/mol.

The H-abstracting ability of each site was investigated by calculating the free energy cost of the following process:

$$Mo_3O_9 + \text{propene} \rightarrow Mo_3O_9H + \text{allyl} \qquad (4)$$

$$Bi_4O_6 + \text{propene} \rightarrow Bi_4O_6H + \text{allyl} \qquad (5)$$

where the C_α–H_α bond of propene is cleaved to produce an allyl radical and an H atom adsorbed on each site. All oxygens are equivalent in the Bi_4O_6 cluster, but there are two different types of oxygens in the Mo_3O_9 cluster – the terminal oxo oxygens and the bridging oxygens. The optimized structure of each cluster with hydrogen adsorbed on each adsorption site is shown in figure 3, and the energy changes are listed in table 3. The energetics for the various reaction steps to be described below are collected together in scheme 2.

3.1.1. Mo site

The energy cost at 673 K (ΔG_{673}) is 27.1 or 42.8 kcal/mol on molybdenum site, depending on whether the dissociated H adsorbs on the terminal oxo oxygen or on the bridging oxygen. Since the dissociation free energy of propene at

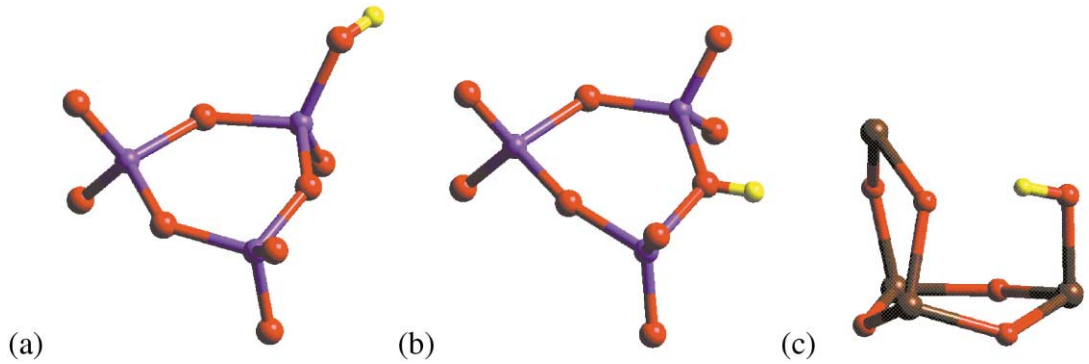

Figure 3. Optimized structures showing a hydrogen adsorbed on (a) an oxo group of Mo_3O_9, (b) a bridging oxygen of Mo_3O_9, and (c) on an oxygen of Bi_4O_6.

Table 3
Energy change (kcal/mol) during H abstraction from propene to each cluster.

	ΔE	ΔZPE	$\Delta\Delta G_{0\to673}$	ΔG_{673}
(a) Mo_3O_9 + propene → Mo_3O_9H (H on O_{oxo}) + allyl	32.9	−2.4	−3.4	27.1
(b) Mo_3O_9 + propene → Mo_3O_9H (H on O_{bridge}) + allyl	50.7	−2.3	−5.6	42.8
(c) Bi_4O_6 + propene → Bi_4O_6H + allyl	50.9	−1.6	−7.6	41.6

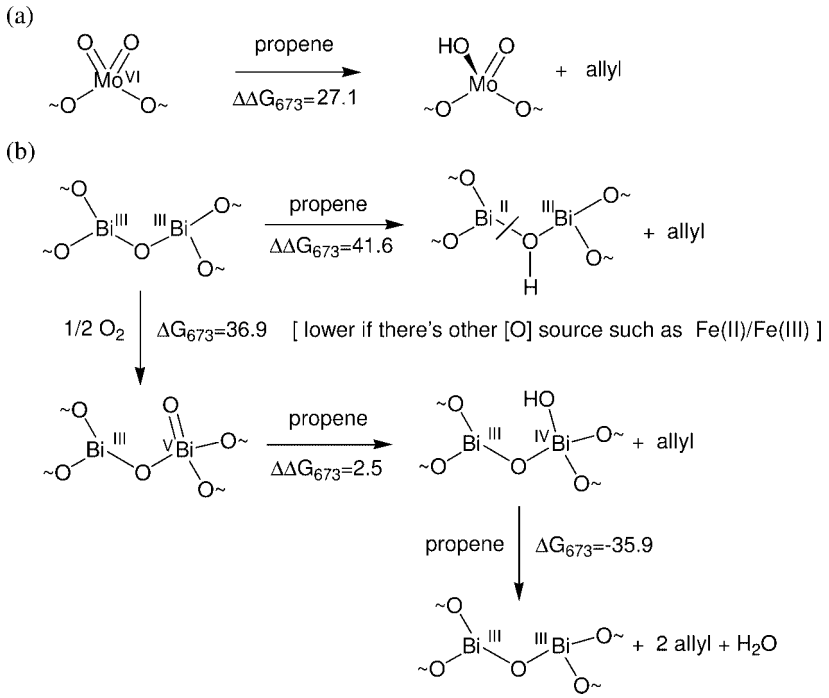

Scheme 2. Summary of the H abstraction from propene by (a) the molybdenum site (implausible) and (b) the bismuth site (plausible only on the oxidized site, which is likely consumed very quickly).

673 K is 69.8 kcal/mol, the binding free energy of hydrogen on Mo_3O_9 is estimated as 42.8 kcal/mol (exothermic) on the terminal oxygen and as 27.0 kcal/mol on the bridging oxygen. The π-bond between Mo and the terminal oxygen is 15 kcal/mol easier to activate than the bond between Mo and the bridging oxygen, so that the terminal oxygen serves as a stronger adsorption site, as proposed from other work [5,42,43]. However, in either case, the H abstraction by Mo_3O_9 is too endothermic to be plausible at 673 K.

3.1.2. Bi(III) site

The corresponding energy cost is 41.6 kcal/mol on bismuth site. (The binding free energy of H on this site is estimated as 28.2 kcal/mol.) This is even more endothermic than on molybdenum site (27.1 kcal/mol), probably because it leads to Bi–O bond cleavage and hence produces a very unfavorable reduced Bi(II) site. This seems contrary to the widely-accepted view that the bismuth site is responsible for the C–H activation of propene.

3.1.3. Bi(V) site

However, bismuth oxide (Bi_2O_3) is known to have a unique ability to chemisorb O_2 dissociatively. Here Bi(III) ($5d^{10}6s^26p^0$) is oxidized to Bi(V) ($5d^{10}6s^06p^0$) [44,45] with the Bi lone pairs responsible for reducing dioxygen. With mixed-valence bismuth oxides, $Bi_{0.7}Ba_{0.3}O_{1.5+\delta}$ [46], and $Bi_{0.6}Y_{0.4}O_{1.5+\delta}$ [47], increasing the effective oxygen partial pressure under preparation conditions (703 K, 5 h), causes a color change from colorless to brown. The excess oxygen introduced under such oxidative conditions oxidize Bi(III) into Bi(V), enabling the charge transfer band from Bi(III) $6s^2$ to Bi(V) $6s^0$, as in other post-transition metallic cation-containing mixed valence oxides (Pb(II)/Pb(IV) or Sb(III)/Sb(V)). Other commercial catalysts for selective oxidation of propene (Fe–Sb–O or U–Sb–O) [48,49] contain antimony (Sb) in place of Bi, which probably plays a similar redox role.

We speculate that in an oxidizing environment an oxygen atom might react with a surface bismuth site, producing a very small amount of Bi(V). This new oxidized site would make H abstraction easier (with simultaneous reduction of Bi(V) to Bi(III)). We calculated the energy cost of (1) producing Bi(V) (Bi_4O_7) from Bi(III) (Bi_4O_6) and (2) abstracting hydrogen from propene by this new active site:

$$Bi_4O_6 + 0.5O_2 \text{ (or other oxygen source)} \rightarrow Bi_4O_7 \quad (6)$$

$$Bi_4O_7 + \text{propene} \rightarrow Bi_4O_7H + \text{allyl} \quad (7)$$

The optimized structures of the oxidized bismuth site and of a hydrogen adsorbed on this site are shown in figure 4, and the energy changes are listed in table 4.

For the defect-like Bi(V) site, the free energy cost to extract the H from propene is just 2.5 kcal/mol. We propose that this oxidized bismuth site is the active site for the H abstraction from propene, as summarized in scheme 2.

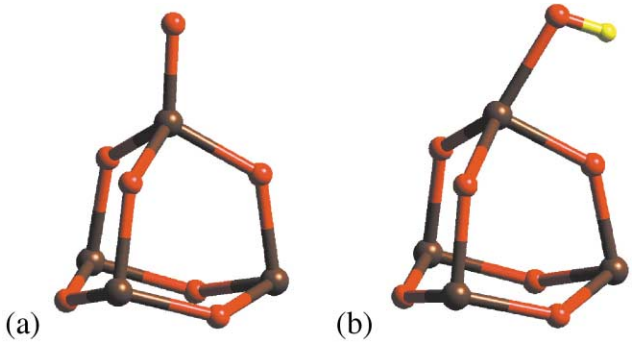

Figure 4. Optimized structures of (a) Bi_4O_7, where a Bi(III) was oxidized to Bi(V) and (b) Bi_4O_7H, where one hydrogen was abstracted from propene to this oxidized Bi(V) site.

On the other hand, the free energy cost for formation of this Bi(V) active site by dissociative chemisorption of gas-phase oxygen molecule is fairly high, 36.9 kcal/mol. Although this is less than 41.6 kcal/mol for the H abstraction by the conventional Bi(III) site, it still seems too high to be plausible. This energy cost includes half the dissociation free energy of oxygen into atomic oxygens. If the gas-phase oxygen molecule is dissociatively chemisorbed at some other site and the resulting atomic oxygen or oxide ion is transported to the Bi(III) site, the energy cost for the formation of active Bi(V) site might be lowered significantly. For example, Fe(II)/Fe(III) is known to serve as an efficient redox couple. The Fe(II) is capable of efficient dioxygen chemisorption and its reductive transformation to lattice oxygen, which can be transferred efficiently to the Bi–O–Mo active site. In fact, drastic improvement in catalyst performance has been achieved by adding Fe(II)/Fe(III). Thus the tetracomponent Mo–Bi–Co–Fe–O catalyst shows the conversion of more than 90% of propene, whereas binary bismuth molybdate (α-$Bi_2Mo_3O_{12}$ and β-$Bi_2Mo_2O_9$) shows the conversion of only about 20% of propene [8]. Indeed it has been suggested that the excellent catalytic activity of this multicomponent catalyst is due to the enhanced activation of oxygen molecule by the Fe(II)/Fe(III) redox couple to atomic lattice oxygen, which migrates to the bismuth site [8].

However, we know of no spectroscopic evidence for the existence of Bi(V) on the bismuth molybdate catalysts. We speculate that this is because, once Bi(V) has been generated, it is consumed and restored to Bi(III) very quickly by reacting with another propene, a very exothermic process (−35.9 kcal/mol):

$$Bi_4O_7H + \text{propene} \rightarrow Bi_4O_6 + H_2O + \text{allyl} \quad (8)$$

3.1.4. MoO_2Cl_2 model

In this section we found that the Mo=O oxo oxygen in molybdate is much more active than the bridging oxygen (Mo–O–Mo). Thus, we expect that the oxo oxygen determines the critical steps of the reactions, making the bridging oxygens spectators that serve to stabilize the presence of the oxo oxygens. Thus, we suspected that the bridging oxygens could be replaced with chlorines as shown in figure 2(c) in calculating the energetics without compromising the results. Replacing the model cluster Mo_3O_9 with MoO_2Cl_2 would make the calculations simpler and faster. To validate this simplification, we calculated the energy changes during sev-

Table 4
Energy change (kcal/mol) during the oxidation of bismuth site and the H abstraction from propene to the oxidized bismuth site.

	ΔE	ΔZPE	$\Delta\Delta G_{0\rightarrow673}$	ΔG_{673}
(a) $Bi_4O_6 + 0.5O_2 \rightarrow Bi_4O_7$	27.5	0.4	9.0	36.9
(b) Bi_4O_7 + propene $\rightarrow Bi_4O_7H$ + allyl	6.4	−2.5	−1.4	2.5
(c) Bi_4O_7H + propene $\rightarrow Bi_4O_6 + H_2O$ + allyl	−14.4	−2.2	−19.3	−35.9

eral key reactions with these two model clusters (the larger one based on Mo_3O_9 and smaller one based on MoO_2Cl_2) (appendix). The simpler model MoO_2Cl_2 gives reasonable energy changes when compared with the more complicated model Mo_3O_9. Thus, the following processes – allyl adsorption and oxygen insertion – were studied with this simpler model, MoO_2Cl_2. We should emphasize here that experimentally, such a simplification could lead to quite different reactions. Using theory we can examine just the chemistry at the oxo groups without considering side reactions that could be induced by the Cl.

3.2. Second step: allyl adsorption

We expect that the allyl radical produced after the H abstraction by the active Bi(V) site is chemisorbed on a nearby active molybdenum or bismuth site. We exclude the possibility that the allyl radical finds another active bismuth site (Bi(V) or Bi(IV)). This is because the concentration of Bi(V) is expected to be very low based on the endothermic oxidation reaction (37.0 kcal/mol), leading to a very low possibility of two adjacent Bi(V) sites. Also a Bi(IV) site is expected to react very quickly with other propenes which are present in much higher amount than allyl radicals, as discussed in section 3.1 (equation (8)).

In order to determine which site is preferable for the allyl adsorption, we calculated the free energy cost of the following processes:

$$\text{allyl} + MoO_2Cl_2 \rightarrow MoO_2Cl_2CH_2CHCH_2 \quad (9)$$

$$\text{allyl} + Bi_4O_6 \rightarrow Bi_4O_6CH_2CHCH_2 \quad (10)$$

There are several possible conformations of the adsorbed allyl group, as shown in figure 5. Only three representative conformations were considered: (a) the conformation where the α-carbon is *cis* with respect to the other oxo group and both α-hydrogens are away from the other oxo group of the molybdenum site (possibly located near to an oxo oxygen of an adjacent site), (b) the conformation where the α-carbon is *cis* with respect to the other oxo group and one of α-hydrogens is *cis* to the other oxo group, and (c) the conformation where the α-carbon is *trans* with respect to the other oxo group. The optimized structures of the allyl-adsorbed clusters are shown in figure 5 and the energy costs are given in table 5.

Again the allyl adsorption on the Bi(III) site results in the Bi–O bond cleavage, producing an unfavorable Bi(II), which

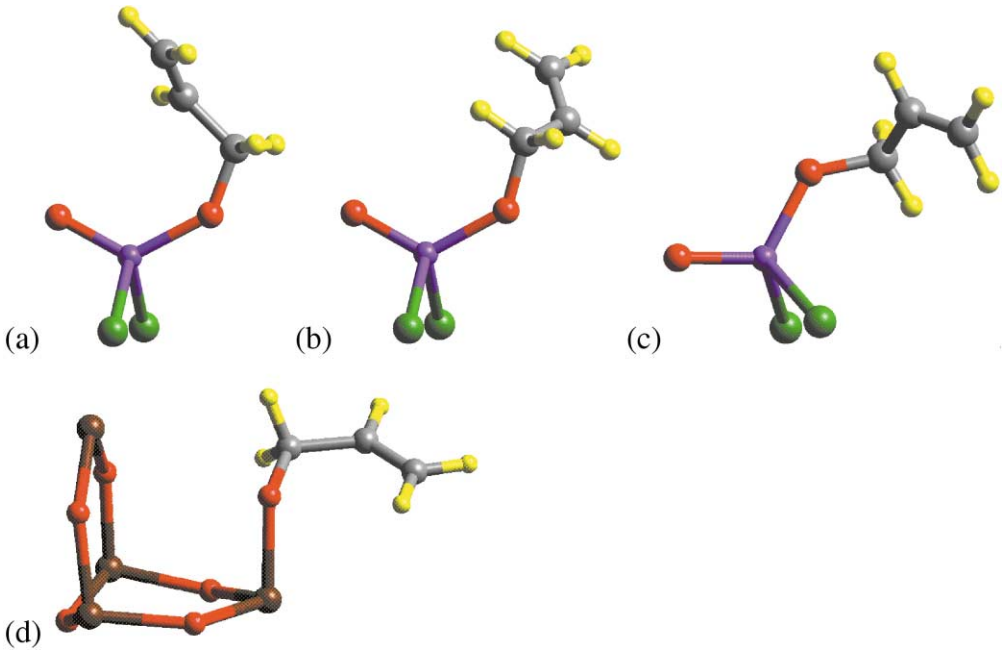

Figure 5. Optimized structures of allyl-adsorbed clusters. (a)–(c) The molybdenum site where the allyl radical is adsorbed in three different conformations (**5a**, **5b**, and **5c**) and (d) the allyl-adsorbed bismuth(III) site.

Table 5
Energy change (kcal/mol) during the adsorption of the allyl radical (a)–(c) on molybdenum site in three different conformations and (d) on bismuth site.

	ΔE	ΔZPE	$\Delta\Delta G_{0\rightarrow 673}$	ΔG_{673}
(a) MoO_2Cl_2 + allyl → $MoO_2Cl_2CH_2CHCH_2$ (**5a**)	−20.5	3.6	23.6	6.7
(b) MoO_2Cl_2 + allyl → $MoO_2Cl_2CH_2CHCH_2$ (**5b**)	−20.3	3.6	23.2	6.5
(c) MoO_2Cl_2 + allyl → $MoO_2Cl_2CH_2CHCH_2$ (**5c**)	−21.5	3.6	23.7	5.7
(d) Bi_4O_6 + allyl → Bi_4O_6_allyl (−41 cm^{-1})	3.8	5.2	22.0	31.0

Table 6
Bond dissociation enthalpies D_{298} (kcal/mol) at 298 K and bond dissociation free energies (kcal/mol) at 673 K of the C–H bonds in the allyl group adsorbed on the molybdenum site ($MoO_2Cl_2C_3H_5$), leading to two different spin states of $MoO_2Cl_2C_3H_4$.

	Leading to singlet		Leading to triplet	
	D_{298}	ΔG_{673}	D_{298}	ΔG_{673}
C_α–H_α	66.1	50.2	67.1	48.1
C_β–H_β	87.7	75.7	107.3	88.1
C_γ–H_γ	–		111.2	91.5

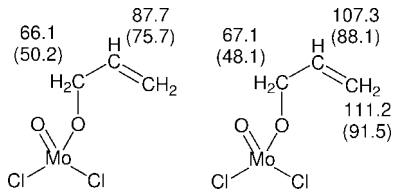

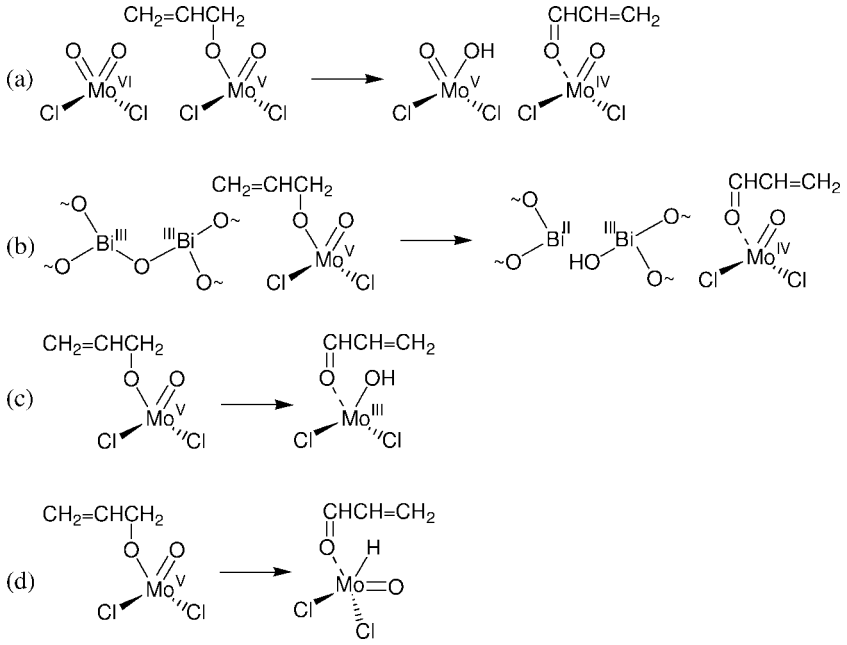

Scheme 3. Several possible pathways of the second H abstraction. The energetics are in table 7.

leads to a high energy cost ($\Delta G_{673\,K} \approx 31$ kcal/mol). However, the adsorption on the terminal oxygen of the molybdenum site needs only moderate energy cost ($\Delta G_{673\,K} =$ 5.7–6.7 kcal/mol) for all three conformations. This indicates that the allyl radical is expected to adsorb preferably at the molybdenum site if a molybdenum site is available near the active bismuth site. This is the case on the bismuth molybdate catalysts (figure 1(c)). In fact, it is consistent with the widely-accepted "dual-site" concept that the allyl group produced on bismuth site adsorbs on molybdenum site [10,11].

On the pure bismuth oxide (α-Bi_2O_3), the only site available for the allyl adsorption after the H abstraction is another bismuth site. The adsorption of the allyl radical on this site is not energetically stable, so that any further reaction other than dimerization of allyl radicals is disfavored. In fact, when propene is passed over α-Bi_2O_3, 1,5-hexadiene and benzene (its cyclization product) are the only major products [10,50,51].

3.3. Third step: second H abstraction and oxygen insertion

The bond dissociation energy was calculated for various C–H bonds in the allyl group chemisorbed on MoO_2Cl_2 (table 6). We find that the C_α–H_α bond ($D_{298} = 66$ kcal/mol) is 21 kcal/mol weaker tha the other CH bonds. Thus, after the allyl radical chemisorbed on one molybdenum site, we expect that a second α-hydrogen is abstracted by a second Mo=O of an adjacent site, producing a precursor of acrolein by simultaneous insertion of the first oxo oxygen into the allyl group.

There are several possible paths for the second α-hydrogen abstraction (scheme 3):

(a) H transfer to an oxo group of an adjacent molybdenum site:

$$MoO_2Cl_2C_3H_5 + MoO_2Cl_2 \rightarrow MoOCl_2\cdots OC_3H_4 + MoO_2Cl_2H \quad (11)$$

(b) H transfer to an oxygen of an adjacent bismuth site:

$$MoO_2Cl_2C_3H_5 + Bi_4O_6 \rightarrow MoOCl_2\cdots OC_3H_4 + Bi_4O_6H \quad (12)$$

(c) H transfer to the other oxo group connected to the same molybdenum:

$$MoO_2Cl_2C_3H_5 \rightarrow MoOHCl_2\cdots OC_3H_4 \text{ or} \quad (13)$$

Table 7
Energy change (kcal/mol) during the second H abstraction.

	ΔE	ΔZPE	$\Delta\Delta G_{0\to673}$	ΔG_{673}
(a) $^2MoO_2Cl_2C_3H_5$ (**5a**) + MoO_2Cl_2 → $^3MoOCl_2\cdots OC_3H_4$ + $^2MoO_2Cl_2H$	12.9	−1.5	−4.6	6.8
$^2MoO_2Cl_2C_3H_5$ (**5c**) + MoO_2Cl_2 → $^3MoOCl_2\cdots OC_3H_4$ + $^2MoO_2Cl_2H$	10.6	−1.5	−4.5	4.6
(b) $^2MoO_2Cl_2C_3H_5$ (**5a**) + Bi_4O_6 → $^3MoOCl_2\cdots OC_3H_4$ + $^2Bi_4O_6H$	30.2	−0.9	−9.4	19.9
$^2MoO_2Cl_2C_3H_5$ (**5c**) + Bi_4O_6 → $^3MoOCl_2\cdots OC_3H_4$ + $^2Bi_4O_6H$	27.9	−0.9	−9.4	17.6
(c) $^2MoO_2Cl_2C_3H_5$ (**5b**) → $^4Mo(OH)Cl_2\cdots OC_3H_4$	21.4	−1.1	−1.7	18.6
(d) $^2MoO_2Cl_2C_3H_5$ (**5c**) → $^2MoHOCl_2\cdots OC_3H_4$	15.8	−2.3	1.0	14.5

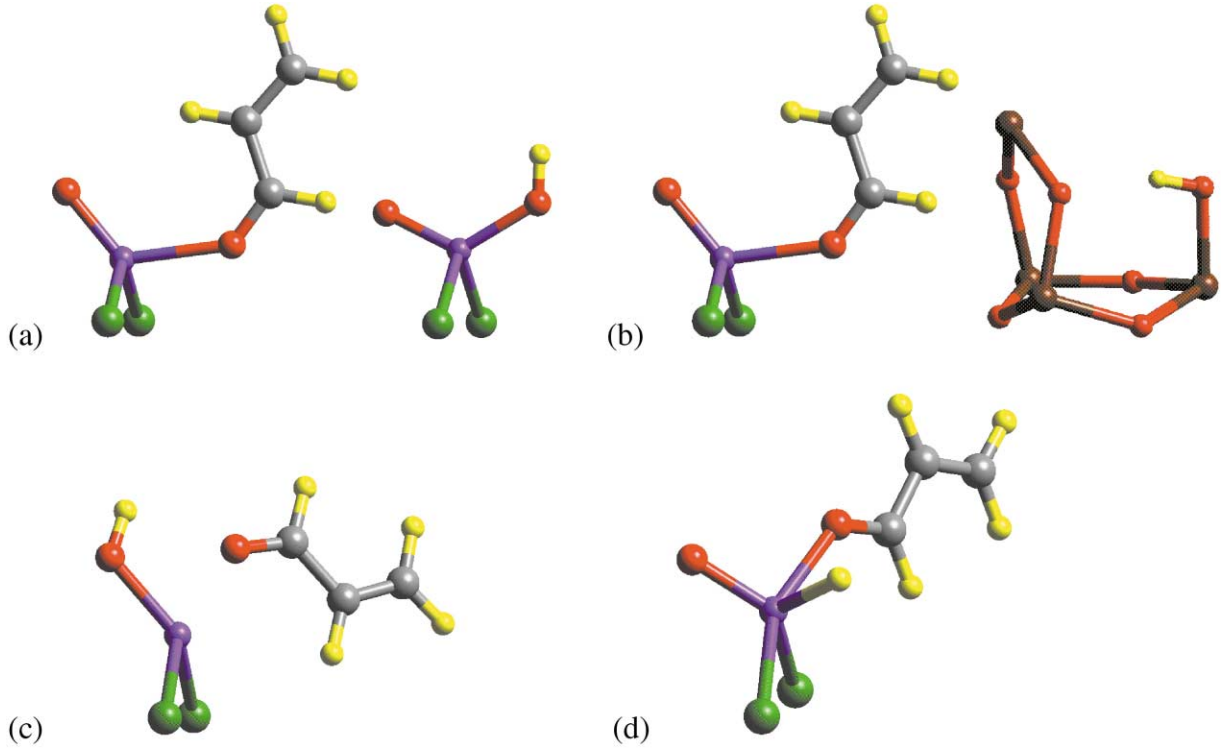

Figure 6. Optimized structures of the intermediate after the second H abstraction. (a)–(b) Two-site transfer schemes starting from **5a**: (a) H transferred to an oxo group of an adjacent molybdenum site, (b) H transferred to an oxygen of an adjacent Bi(III) site. (c) Single-site transfer scheme starting from **5b**: H transferred to the other oxo group, and (d) single-site transfer scheme starting from **5c**: H transferred to the molybdenum center. Note that we show the most favorable structure of the products, while the reaction pathway might go through other intermediates on the way to this structure.

(d) H transfer to the molybdenum center:

$$MoO_2Cl_2C_3H_5 \rightarrow MoHOCl_2\cdots OC_3H_4 \qquad (14)$$

Pathways (1) and (2) are accessible for conformations **5a** and **5c**, pathway (3) for **5b**, and pathway (4) for **5c**. Again we exclude the possibility that the hydrogen is abstracted by another active bismuth site (Bi(V) or Bi(IV)) as discussed in section 3.2.

The calculated free energy cost necessary for each path is given in table 7. We find that the most favorable mechanism for extracting the second hydrogen is path (a), to an oxo group of the adjacent molybdenum site (two-site scheme; ΔG_{673} = 4.6 kcal/mol from **5c** or 6.8 kcal/mol from **5a**). Thus we expect that at least two adjacent molybdenum sites are necessary for the most favorable reaction, as suggested by Allison and Goddard [5]. Indeed some of the bismuth molybdate catalysts have this structure in the bulk phase (e.g., α-$Bi_2Mo_3O_{12}$ [13,14], shown schematically in figure 1(c)) while in others it may be introduced in the surface.

3.4. Fourth step: acrolein desorption

After the second H abstraction, there are two likely possibilities in further reactions of $MoOCl_2\cdots OC_3H_4$:

(1) desorption of the acrolein or

(2) the third H abstraction.

The desorption of acrolein is exothermic (table 8(a)). Acrolein can desorb easily at this stage, leaving behind $^3MoOCl_2$ (figure 7). On the other hand, the energy cost of further C_α–H_α activation is so high (table 8(b)) that the third α-H abstraction is not likely to happen.

3.5. Reoxidation

The reduced Mo(IV) site ($MoOCl_2$) left behind the acrolein desorption must be reoxidized in order to regain the intial state:

$$MoOCl_2 + 0.5O_2 \text{ (or other oxygen source)} \rightarrow MoO_2Cl_2 \quad (15)$$

The Mo(V) sites ($MoO(OH)Cl_2$) produced by abstracting hydrogen from allyl groups adsorbed on adjacent molybdenum sites (section 3.3) can be reoxidized through dehydration:

$$2MoO(OH)Cl_2 + 0.5O_2 \text{ (or other oxygen source)} \rightarrow 2MoO_2Cl_2 + H_2O \quad (16)$$

The energy changes during these processes are given in table 9. Again, there might be other sources of atomic oxygen species (e.g., lattice oxygen) that would change the energy cost shown in table 9. In any case, this reoxidation of molybdenum is very exothermic. We speculate that this exothermic reoxidation of molybdenum site could be coupled with the oxidation of bismuth site from Bi(III) to Bi(V).

Figure 7. Model cluster $MoOCl_2$ representing the reduced molybdenum site Mo(IV).

This exothermic reoxidation of molybdenum site could be a driving force to draw lattice oxygens generated remotely, placing them nearby a bismuth, which would favor oxidizing the Bi.

3.6. Summary: oxidation

The reaction mechanism with the most favorable energetics (through conformation **5c**) is summarized in schemes 4 and 5. The final reaction equation is:

$$CH_3CHCH_2 + O_2 \rightarrow CH_2CHCHO + H_2O$$
$$\Delta G_{673} = -74.0 \text{ kcal/mol } (-72.8 \text{ kcal/mol at 298 K}).$$

4. Ammoxidation

For ammoxidation we investigated (1) ammonia activation on a molybdenum site to generate imido groups and (2) allyl adsorption on these imido sites. Since the H abstraction from propene is believed to occur on bismuth site, we assumed that this process is not affected by the presence of ammonia and did not investigate this step again.

4.1. Ammonia activation

First we calculated the energetics of each step involved in ammonia activation on a single molybdenum site. The

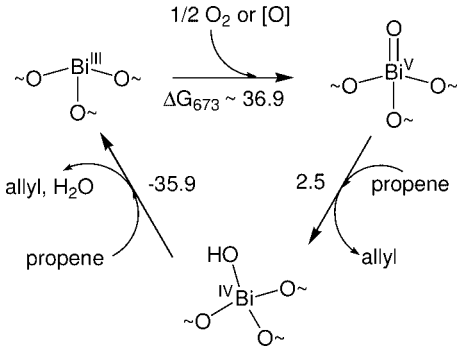

Scheme 4. Oxidation part 1. Hydrogen abstraction on bismuth site.

Table 8
Energy change (kcal/mol) during (a) desorption of acrolein and (b)–(c) third H abstraction.

	ΔE	ΔZPE	$\Delta\Delta G_{0\rightarrow673}$	ΔG_{673}
(a) $^3MoOCl_2\cdots OC_3H_4$ (from **5a**) $\rightarrow$ $^3MoOCl_2 + {}^1CH_2CHCHO$	17.2	−1.6	−25.2	−9.6
$^3MoOCl_2\cdots OC_3H_4$ (from **5c**) $\rightarrow$ $^3MoOCl_2 + {}^1CH_2CHCHO$	20.5	−1.5	−25.4	−6.4
(b) $^3MoOCl_2\cdots OC_3H_4$ (from **5c**) $+ MoO_2Cl_2$ $\rightarrow$ $^2MoOCl_2\cdots OCCHCH_2 + {}^2MoO_2Cl_2H$	49.3	−2.0	−4.1	43.1
$^3MoOCl_2\cdots OC_3H_4$ (from **5a**) $+ MoO_2Cl_2$ $\rightarrow$ $^2MoOCl_2\cdots OCCHCH_2 + {}^2MoO_2Cl_2H$	43.7	−2.0	−3.2	38.5

Table 9
Energy change (kcal/mol) during the reoxidation.

	ΔE	ΔZPE	$\Delta\Delta G_{0\rightarrow673}$	ΔG_{673}
$MoOCl_2 + 0.5O_2 \rightarrow MoO_2Cl_2$	−68.5	1.3	14.4	−52.8
$2MoO(OH)Cl_2 + 0.5O_2 \rightarrow 2MoO_2Cl_2 + H_2O$	−47.6	0.1	−6.2	−53.7

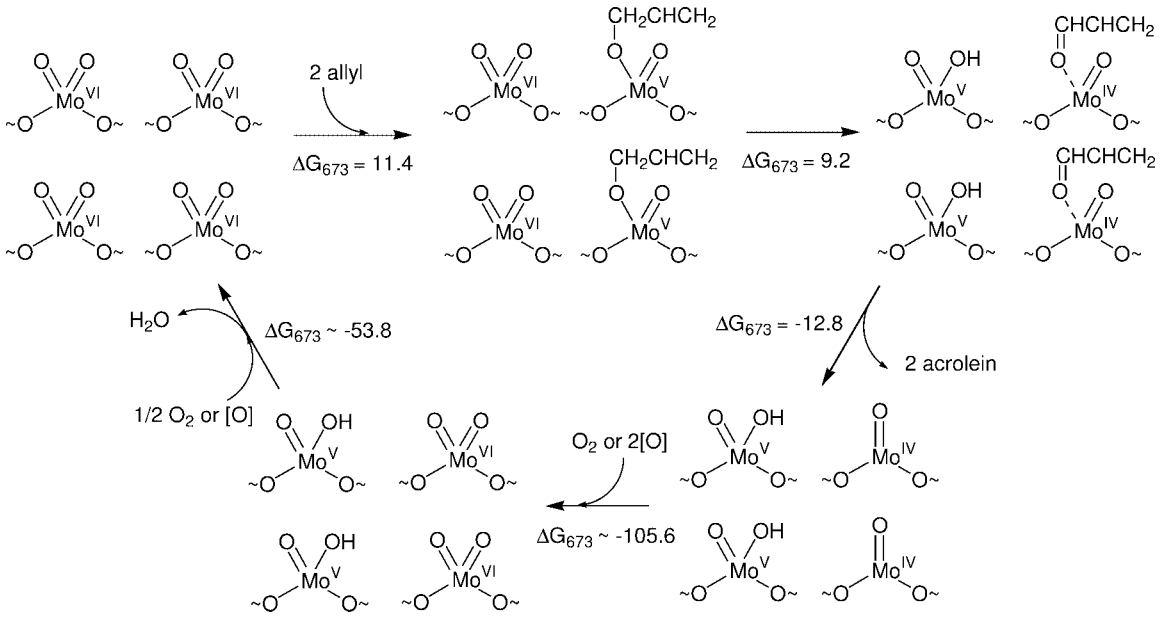

Scheme 5. Oxidation part 2. Allyl adsorption, oxygen insertion, and reoxidation on molybdenum site.

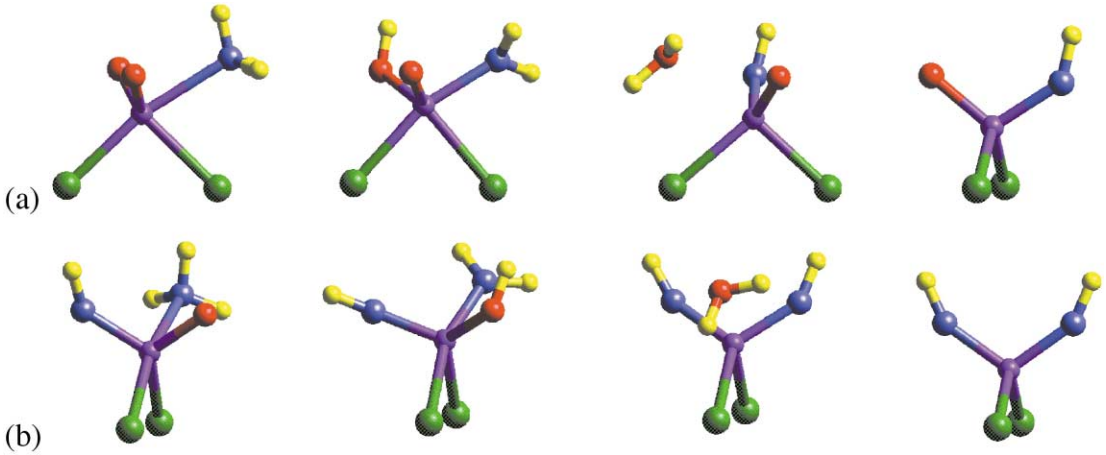

Figure 8. Optimized structures for intermediates during ammonia activation on MoO_2Cl_2. (a) Activation of the first ammonia to generate $MoO(NH)Cl_2$ and (b) activation of the second ammonia to generate $Mo(NH)_2Cl_2$.

most abundant molybdenum species is Mo(VI), and this was represented by a model cluster MoO_2Cl_2 (figure 2(c)). The activation of the first ammonia would proceed via

(1) ammonia adsorption on MoO_2Cl_2,

(2) hydrogen transfers from ammonia to an oxo group, and

(3) desorption of water leaving behind the imido group, $MoO(NH)Cl_2$.

The activation of the second ammonia would proceed in the same way starting from $MoO(NH)Cl_2$ and ending up with $Mo(NH)_2Cl_2$. The optimized structures of possible intermediates are shown in figure 8 and the energy changes are given in table 10. The activation process of the first ammonia is summarized in scheme 6.

The overall energy cost (ΔG_{673}) is 12.4 kcal/mol for the first ammonia activation and 15.4 kcal/mol for the second ammonia activation. The processes are quite endothermic and the second activation is harder than the first one. The ammonia adsorption is not easy ($\Delta G_{673} = 8.9$ for the first ammonia and 13.1 kcal/mol for the second ammonia), and the first hydrogen transfer from the adsorbed ammonia to an adjacent oxo group costs as much as 26 kcal/mol for both cases. These processes seem too endothermic to be plausible.

Since ammonia is a well-known reducing agent, there might be a significant amount of reduced molybdenum sites in the presence of ammonia. The presence of propene could also generate reduced molybdenum sites, Mo(IV), in the course of its oxidation to acrolein, prior to ammoxidation. We speculated that the ammonia activation could be easier on this reduced Mo(IV) site which can be represented by $MoOCl_2$ (figure 7). This is because this site has one open adsorption site, making the ammonia adsorption easier than

Table 10
Energy change (kcal/mol) during ammonia activation on Mo(VI) represented as MoO_2Cl_2.

	ΔE	ΔZPE	$\Delta\Delta G_{0\to673}$	ΔG_{673}
(a) 1st ammonia activation to generate $MoO(NH)Cl_2$				
$MoO_2Cl_2 + NH_3 \to MoO_2Cl_2\cdots NH_3$	−16.7	3.1	22.5	8.9
$MoO_2Cl_2\cdots NH_3 \to MoO(OH)Cl_2(NH_2)$	28.8	−2.0	−0.5	26.3
$MoO(OH)Cl_2(NH_2) \to MoO(NH)Cl_2\cdots OH_2$	−4.5	−0.1	−0.1	−4.7
$MoO(NH)Cl_2\cdots OH_2 \to MoO(NH)Cl_2 + H_2O$	6.1	−2.4	−21.8	−18.1
(net) $MoO_2Cl_2 + NH_3 \to MoO(NH)Cl_2 + H_2O$	13.7	−1.4	0.1	12.4
(b) 2nd ammonia activation to generate $Mo(NH)_2Cl_2$				
$MoO(NH)Cl_2 + NH_3 \to MoO(NH)Cl_2\cdots NH_3$	−13.5	3.0	23.7	13.1
$Mo(NH)Cl_2\cdots NH_3 \to Mo(OH)(NH)Cl_2(NH_2)$	28.7	−2.0	−0.7	26.0
$Mo(OH)(NH)Cl_2(NH_2) \to Mo(NH)_2Cl_2\cdots OH_2$	−1.6	−0.4	−1.1	−3.1
$Mo(NH)_2Cl_2\cdots OH_2 \to Mo(NH)_2Cl_2 + H_2O$	2.8	−2.2	−21.1	−20.6
(net) $MoO(NH)Cl_2 + NH_3 \to Mo(NH)_2Cl_2 + H_2O$	16.4	−1.6	0.8	15.4

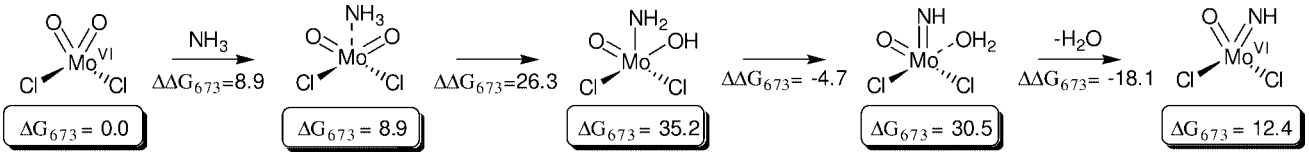

Scheme 6. Activation of the first ammonia to generate $MoO(NH)Cl_2$ from Mo(VI) represented as MoO_2Cl_2.

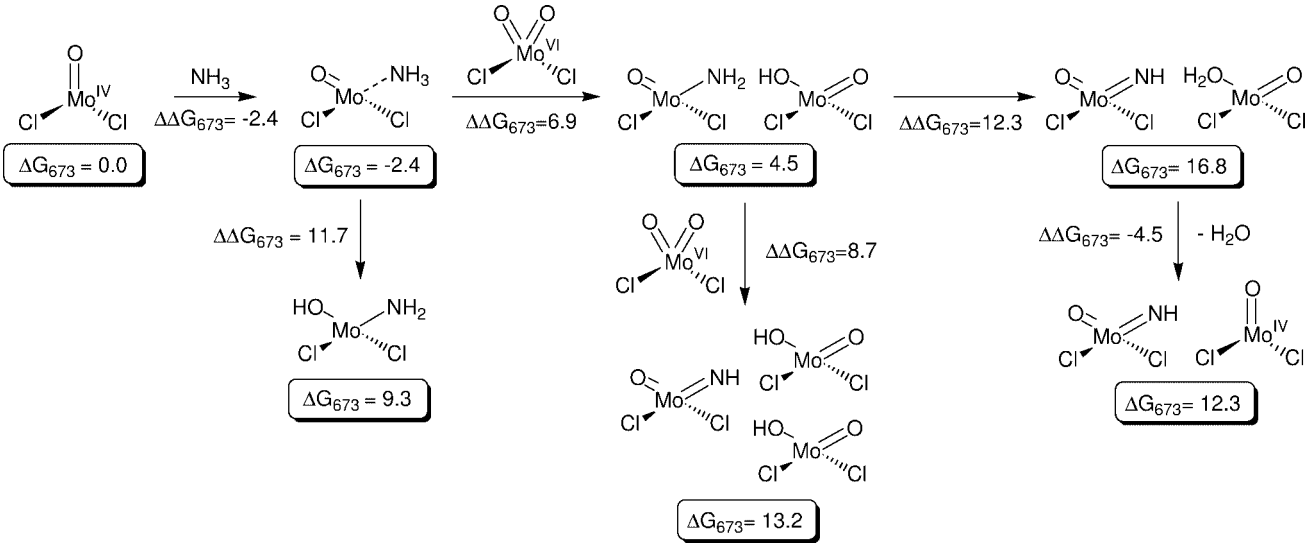

Scheme 7. Activation of the first ammonia on Mo(IV) represented as $MoOCl_2$.

on MoO_2Cl_2. Moreover, whereas one of the oxo groups should be removed from $MoO_2Cl_2\cdots NH_3$ and the hydrogen transfer from ammonia should be intramolecular in the ammonia activation involving Mo(VI) site (figure 8), the oxo group would not have to be removed from $MoOCl_2\cdots NH_3$ in the ammonia activation involving Mo(IV) site and the hydrogen could be transfered from ammonia to an oxo group of an adjacent molybdenum site (scheme 7), making this process easier. Thus, we calculated the energetics of ammonia activation on a reduced molybdenum site Mo(IV): (1) the ammonia adsorption on $MoOCl_2$ and (2) hydrogen transfer from ammonia to an oxo group of an adjacent molybdenum site (table 11).

The net energy cost is the same (12.3 kcal/mol), but the energy cost of each step was reduced greatly for Mo(IV). As expected, the ammonia adsorption is now exothermic (−2.4 kcal/mol) on Mo(IV) and the first hydrogen transfer costs only 6.9 kcal/mol by the aid of an adjacent molybdenum site. The second hydrogen transfer is now the least favorable (rate-determining) step, and the energy cost (12.3 kcal/mol) is much smaller than the 26 kcal/mol of the rate-determining step on Mo(VI). This energy cost could be reduced even more to 8.7 kcal/mol, if one more adjacent molybdenum site is present nearby with its oxo group playing a role as a second hydrogen acceptor. These results indicate that ammonia activation is much easier under reducing

Table 11
Energy change (kcal/mol) during ammonia activation on Mo(IV) represented as $MoOCl_2$.

(a) 1st ammonia activation to generate $MoO(NH)Cl_2$	ΔE	ΔZPE	$\Delta\Delta G_{0\to673}$	ΔG_{673}
$MoOCl_2 + NH_3 \rightarrow MoOCl_2\cdots NH_3$	−28.5	2.9	23.2	−2.4
$MoOCl_2\cdots NH_3 + MoO_2Cl_2 \rightarrow MoOCl_2(NH_2) + MoO(OH)Cl_2$	10.1	−2.1	−1.1	6.9
$MoOCl_2(NH_2) + MoO(OH)Cl_2$ $\rightarrow MoO(NH)Cl_2 + MoOCl_2\cdots OH_2^*$	12.2	0.2	−0.2	12.3
$MoOCl_2\cdots OH_2 \rightarrow MoOCl_2 + H_2O$	19.8	−2.5	−21.8	−4.5
(net) $MoO_2Cl_2 + NH_3 \rightarrow MoO(NH)Cl_2 + H_2O$	13.6	−1.5	0.1	12.3

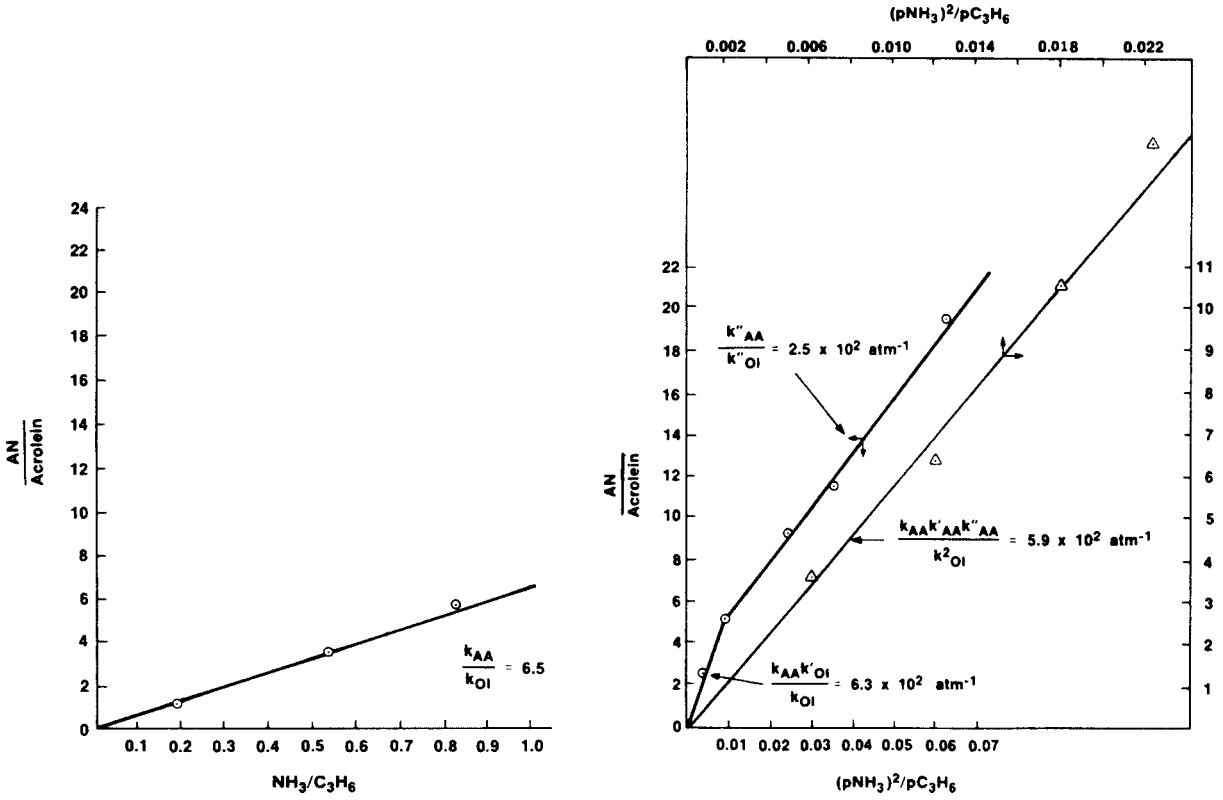

(a) (b)

Figure 9. Relationship between the ammonia/propene feed ratio and the acrylonitrile/acrolein product ratio. This depends on the partial pressure of reactants in the feed. (a) Low feed pressure ($p(C_3H_6) = 0.041$ atm) and (b) intermediate feed pressure ($p(C_3H_6) = 0.082$ atm; dual-slope line) and high feed pressure ($p(C_3H_6) = 0.14$ atm; single-slope line). Burrington, Kartisek and Grasselli [52].

conditions, for example, at higher partial pressures of ammonia and propene.

These results are consisitent with experimental findings of Grasselli and coworkers on the kinetic behavior of ammonia activation and their interpretation [52]. From a kinetic study on the ammoxidation process, Grasselli and coworkers found that the relationship between the ammonia/propene feed ratio and the acrylonitrile/acrolein product ratio depends on the partial pressure of reactants in the feed (figure 9). At low partial pressures of feed ($p(C_3H_6) = 0.041$ atm), the product ratio is a linear function of NH_3/C_3H_6, indicating that one ammonia molecule is involved at the N-insertion site per catalytic cycle. At intermediate and high partial pressures of feed ($p(C_3H_6) =$ 0.082 and 0.14 atm), the product ratio is a linear function of $(NH_3)^2/C_3H_6$, corresponding to two ammonia molecules activated at the N-insertion site per acrylonitrile formed.

They interpreted this by assuming different active sites at different partial pressures of feed (scheme 8). At low partial pressures of feed ($p(C_3H_6) = 0.041$ atm), the major surface species involved in N insertion is a low concentration of "oxo–imido" species surrounded by abundant "oxo–oxo"species (**8** in scheme 8). At intermediate partial pressures of feed ($p(C_3H_6) = 0.082$ atm), it is a high concentration of "oxo–imido" species which are now present next to each other (**9** in scheme 8). At higher partial pressures of feed ($p(C_3H_6) = 0.14$ atm), "imido–imido" species (**10** in scheme 8) are the major N-inserting species. That is, "imido" groups generated by the ammonia activation are more abundant in higher partial pressure of feeds (ammonia and propene), that is, in more reducing conditions. Our calculations lead to independent confirmation of this interpretation.

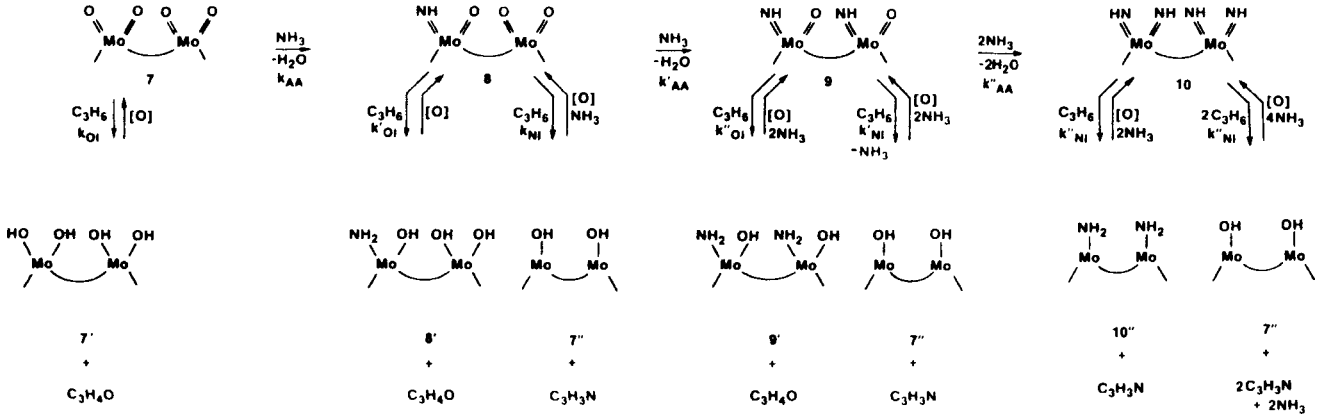

Scheme 8. Model of activation of ammonia and propene over molybdate, proposed by Grasselli and coworkers. Burrington, Kartisek and Grasselli [52].

Table 12
Energy change (kcal/mol) during the adsorption of an allyl radical on various molybdenum sites.

	ΔE	ΔZPE	$\Delta\Delta G_{0\to673}$	ΔG_{673}
(a) MoO_2Cl_2 + allyl → $MoO_2Cl_2\cdots$allyl	−21.5	3.6	23.7	5.7
(b) $MoO(NH)Cl_2$ + allyl → $MoO(NH)Cl_2\cdots$allyl (allyl on oxo)	−34.3	4.8	25.5	−4.0
(c) $MoO(NH)Cl_2$ + allyl → $MoO(NH)Cl_2\cdots$allyl (allyl on imido)	−14.4	3.3	23.8	12.8
(d) $Mo(NH)_2Cl_2$ + allyl → $Mo(NH)_2Cl_2\cdots$allyl	−26.5	4.3	25.1	2.9

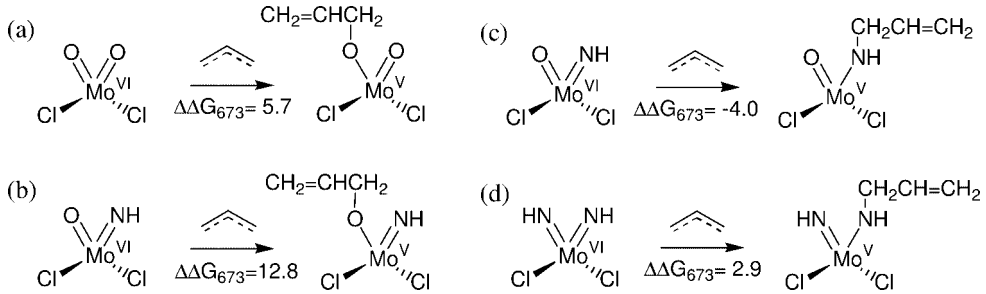

Scheme 9. Allyl adsorption on various molybdenum sites.

4.2. Allyl adsorption

In table 12 and scheme 9 we show the calculated energetics for adsorption of an allyl radical (a) of the oxo group of "oxo–oxo" (discussed in the section on oxidation), (b) the imido group of the "oxo–imido" species, (c) the oxo group of the "oxo–imido" species, and (d) an imido group of the "imido–imido" species.

Comparing (a) with (c), we can see that the allyl adsorption is 10 kcal/mol more favorable on an imido group than on an oxo group for an oxo spectator group. Similarly comparing (b) with (d) we also find that allyl adsorption is 10 kcal/mol more favorable on an imido group than on an oxo group for an imido spectator group.

Comparing (a) and (b), where the allyl adsorbs on the same oxo group, indicates that the spectator effect of an oxo group is 7 kcal/mol larger than that of an imido group. Similarly comparing (b) and (d) we find that when the allyl adsorbs on the same imido group, the spectator effect of an oxo group is 7 kcal/mol larger than that of an imido group.

$$\frac{r(C_3H_3N)}{r(C_3H_4O)} = \frac{k'_{NI}(\mathbf{9})(C_3H_6)}{k_{PA}(\mathbf{7})(C_3H_6) + k''_{PA}(\mathbf{9})(C_3H_6)}. \quad (19)$$

At steady-state conditions for **9**,

$$k'_{NI}(\mathbf{9})(C_3H_6) + k''_{OI}(\mathbf{9})(C_3H_6) = k_{AA}k'_{AA}(NH_3)^2(\mathbf{7}) \quad (20)$$

and assuming that N insertion is again favored over O insertion, $k'_{NI} \gg k''_{OI}$, and that $k_{OI}(\mathbf{7}) \gg k'_{OI}(\mathbf{9})$ over this region, equation (19) reduces to

$$\frac{r(C_3H_3N)}{r(C_3H_4O)} = \frac{k_{AA}k'_{AA}(NH_3)^2}{k_{OI}(C_3H_6)}. \quad (4)$$

Figure 10. Assumptions made to derive a kinetic equation for ammoxidation. Burrington, Kartisek and Grasselli [52].

These results are consistent with the assumption that Grasselli and coworkers made to derive kinetic equations for

ammoxidation (figure 10). They assumed that "N insertion is favored over O insertion, $k'_{NI} >> k''_{OI}$". Considering that the allyl adsorption is the major part of the O- or N-insertion process, the lower energy cost for the allyl adsorption on an imido group (case (b); −4.0 kcal/mol) than on an oxo group (case (c); 12.8 kcal/mol) confirms this assumption. They also assumed that "O insertion from di-oxo is easier than from oxo–imido, $k_{OI} >> k'_{OI}$". Lower energy cost for the allyl adsorption on an oxo group of the "oxo–oxo" species (case (a); 5.7 kcal/mol) than on an oxo group of the "oxo–imido" species (case (c); 12.8 kcal/mol) confirms this assumption.

Another implication from these calculations is that the most favorable site for ammoxidation would be the "oxo–imido" one. The allyl adsorption on the imido group of this site was the most favorable among various adsorption possibilities.

4.3. Summary: ammoxidation

Our calculation indicated that ammonia activation would be easier on Mo(IV) rather than on Mo(VI). Ammonia would be activated more easily for more reducing condition. Since ammonia and propene are reducing agents, higher partial pressures of them could accelerate the ammonia activation. This is consistent with the kinetic model of ammoxidation proposed by Grasselli and coworkers that imido sites

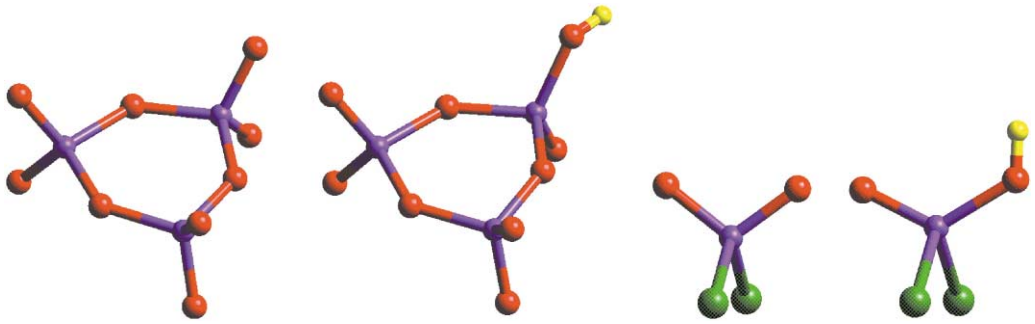

Figure 11. Mo_3O_9 vs. MoO_2Cl_2. H adsorption on the oxo oxygen.

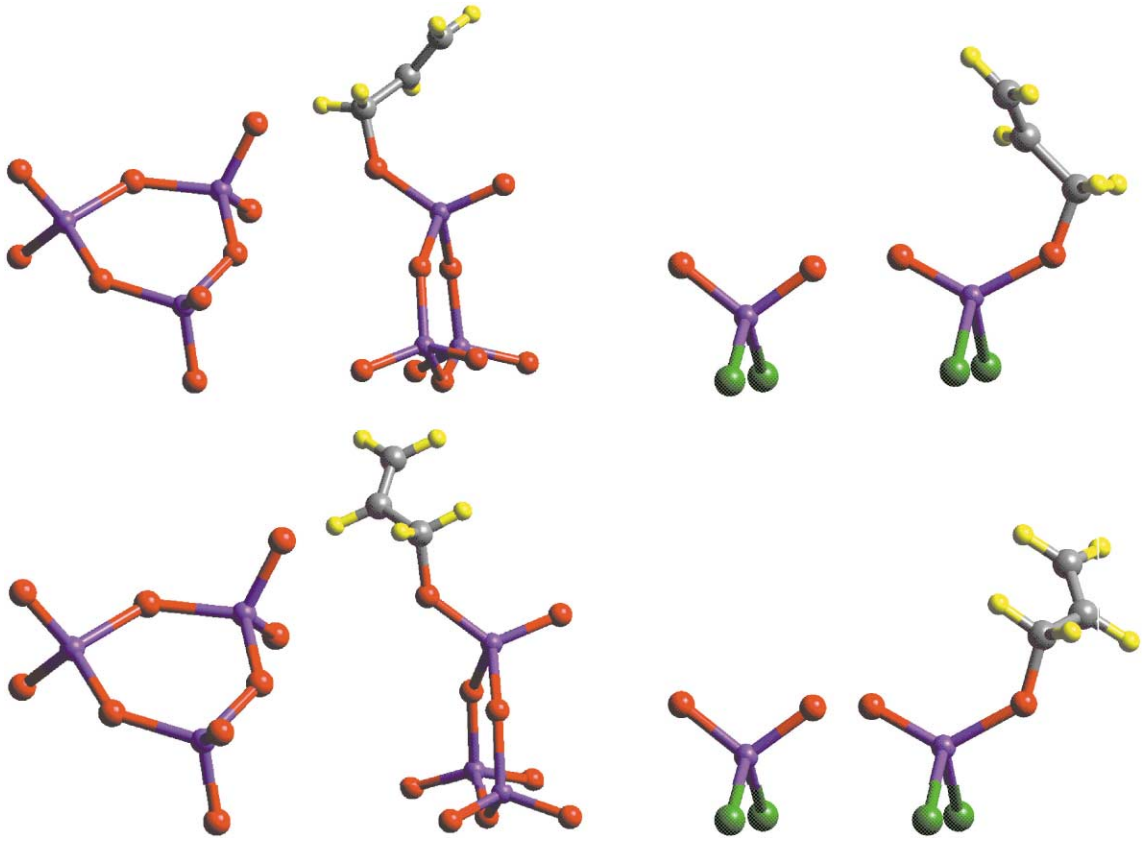

Figure 12. Mo_3O_9 vs. MoO_2Cl_2. Allyl adsorption on an oxo oxygen in two different conformations.

Figure 13. Mo_3O_9 vs. MoO_2Cl_2. Re-oxidation.

Table 13
Mo_3O_9 vs. MoO_2Cl_2. H adsorption on the oxo oxygen.

	ΔE	ΔZPE	$\Delta\Delta G_{0\to673}$	ΔG_{673}
Mo_3O_9 + propene → Mo_3O_9_H + allyl	32.9	−2.4	−3.4	27.1
MoO_2Cl_2 + propene → MoO_2Cl_2_H + allyl	34.4	−2.1	−2.5	29.8

Table 14
Mo_3O_9 vs. MoO_2Cl_2. Allyl adsorption on an oxo oxygen in two different conformations.

	ΔE	ΔZPE	$\Delta\Delta G_{0\to673}$	ΔG_{673}
Mo_3O_9 + allyl → Mo_3O_9_allyl (upper)	−21.3	?	?	?
MoO_2Cl_2 + allyl → MoO_2Cl_2_allyl (upper)	−20.5	3.6	23.6	6.7
Mo_3O_9 + allyl → Mo_3O_9_allyl (lower)	−21.4	?	?	?
MoO_2Cl_2 + allyl → MoO_2Cl_2_allyl (lower)	−20.3	3.6	23.2	6.5

(Mo=NH) are more abundant in higher partial pressures of feed.

Our calculations also indicate that allyl groups produced as a result of the hydrogen abstraction from propenes would be adsorbed more easily on imido groups (Mo=NH) than on oxo groups (Mo=O) and that the spectator oxo effect is larger than spectator imido effect. Thus, we propose that the best site for ammoxidation (at least for allyl adsorption) is the imido group of the "oxo–imido" species.

Acknowledgement

We thank Asahi Chemical Ind. Co., Ltd., Fuji, Shizuoka 416–8501, Japan for providing funding for this project and Dr. Terumasa Yamasaki of Asahi Chemical for helpful comments. We also thank Dr. Bob Grasselli and Dr. Jim Burrington for many helpful discussions over the years. The facilities of the MSC are also supported by grants from NSF-MRI, DOE-ASCI, ARO/MURI, Chevron, 3M, Beckman Institute, Seiko-Epson, Dow, Avery-Dennison, Kellogg, NSF-CHE, NIH, and ARO/DURIP.

Appendix. Mo_3O_9 versus MoO_2Cl_2

In section 3.1 we found that the terminal oxo oxygens (=O) in Mo_3O_9 are much more active than the bridging oxygens (–O–). This suggests that the reactions can be described by including only oxo oxygens in the model (no bridging oxygens). Thus, to simplify and reduce the costs of the calculations, we replaced the bridging oxygens with chlorines (MoO_2Cl_2). In order to determine the effect of this replacement, we calculated the energy changes involved in several key reactions on these two model clusters: (1) H adsorption, (2) allyl adsorption in two different conformations, and (3) re-oxidation from Mo(IV) to Mo(VI) (tables 13–15 and figures 11–13). The energy changes calculated using the simple MoO_2Cl_2 model are quite similar to those calculated on the more complicated Mo_3O_9 model. This validates the use of the simple MoO_2Cl_2 model.

Table 15
Mo_3O_9 vs. MoO_2Cl_2. Re-oxidation.

	ΔE	ΔZPE	$\Delta\Delta G_{0\to673}$	ΔG_{673}
$Mo_3O_8 + 0.5O_2 \to Mo_3O_9$	−72.9	1.5	15.3	−56.1
$MoOCl_2 + 0.5O_2 \to MoO_2Cl_2$	−68.5	1.3	14.4	−52.8

References

[1] A.K. Rappé and W.A. Goddard III, Nature 285 (1980) 311.
[2] A.K. Rappé and W.A. Goddard III, J. Am. Chem. Soc. 102 (1980) 5114.
[3] A.K. Rappé and W.A. Goddard III, J. Am. Chem. Soc. 104 (1982) 448.
[4] A.K. Rappé and W.A. Goddard III, J. Am. Chem. Soc. 104 (1982) 3287.
[5] J.N. Allison and W.A. Goddard III, in: *Active Sites on Molybdenum Surfaces, Mechanistic Considerations for Selective Oxidation*

and Ammoxidation of Propene, Vol. 279, eds. R.K. Grasselli and J.F. Bradzil (Am. Chem. Soc., Washington, DC, 1985) pp. 23–36.
[6] G.W. Hearne and M. Adams, Shell Development Co., US Patent 2 (1948) Vol. 451, p. 485.
[7] J.D. Idol, Standard Oil, Co., Ohio (SOHIO), US Patent 2 (1959) Vol. 904, p. 580.
[8] Y. Moro-Oka and W. Ueda, Adv. Catal. 40 (1994) 233.
[9] R.K. Grasselli, J.D. Burrington and J.F. Brazdil, Faraday Discussions 72 (1981) 203.
[10] J. Habor and B. Grzybowska, J. Catal. 28 (1973) 489.
[11] J.D. Burrington, C.T. Kartisek and R.K. Grasselli, J. Catal. 81 (1983) 489.
[12] L. Kihlborg, Arkiv Kemi 21 (1963) 357.
[13] H.A. Harwig, Anorg. Allg. Chem. 444 (1978) 151.
[14] A.F. van den Elzen and G.D. Rieck, Acta Cryst. B 29 (1973) 2433.
[15] F. Theobald and A. Laarif, Mater. Res. Bull. 20 (1985) 653.
[16] J. Berkowitz, M.G. Inghram and W.A. Chupka, J. Chem. Phys. 26 (1957) 842.
[17] S. Maleknia, J. Brodbelt and K. Pope, J. Am. Soc. Mass Spectrosc. 2 (1991) 212.
[18] E.F. Fialko, A.V. Kikhtenko, V.B. Goncharov and K.I. Zamaraev, J. Phys. Chem. A 101 (1997) 8607.
[19] M.R. France, J.W. Buchanan, J.C. Robinson, S.H. Pullins, J.L. Tucker, R.B. King and M.A. Duncan, J. Phys. Chem. A 101 (1997) 6214.
[20] L.N. Sidorov, I.I. Minayeva, E.Z. Zasorin, I.D. Sorokin and A.Y. Borshchevskiy, High Temp. Sci. 12 (1980) 175.
[21] M. Bienati, V. Bonacic-Koutecky and P. Fantucci, J. Phys. Chem. A 104 (2000) 6983.
[22] E. Oniyama and P.G. Wahlbeck, J. Phys. Chem. B 102 (1998) 4418.
[23] A. Fielicke and K. Rademann, J. Phys. Chem. A 104 (2000) 6979.
[24] M. Kinne, A. Heidenreich and K. Rademann, Angew. Chem. Int. Ed. 37 (1998) 2509.
[25] M. Kinne and K. Rademann, Chem. Phys. Lett. 284 (1998) 363.
[26] J.C. Slater, *Quantum Theory of Molecules and Solids*, Vol. 4, *The Self-Consistent Field for Molecules and Solids* (McGraw-Hill, New York, 1974).
[27] A.D. Becke, Phys. Rev. A 38 (1988) 3098.
[28] S.H. Vosko, L. Wilk and M. Nusair, Canad. J. Phys. 58 (1980) 1200.
[29] C.T. Lee, W.T. Yang and R.G. Parr, Phys. Rev. B 37 (1988) 785.
[30] B. Miehlich, A. Savin, H. Stoll and H. Preuss, Chem. Phys. Lett. 157 (1989) 200.
[31] T.H. Dunning, Jr., J. Chem. Phys. 90 (1989) 1007.
[32] R.A. Kendall, T.H. Dunning, Jr. and R.J. Harrison, J. Chem. Phys. 96 (1992) 6796.
[33] P.J. Hay and W.R. Wadt, J. Chem. Phys. 82 (1985) 299.
[34] Jaguar 3.5, Schrodinger Inc.: Portland, OR (1998).
[35] B.H. Greeley, T.V. Russo, D.T. Mainz, R.A. Friesner, J.-M. Langlois, W.A. Goddard III, R.E. Donnelly and M.N. Ringalda, J. Chem. Phys. 101 (1994) 4028.
[36] *CRC Handbook of Chemistry and Physics*, 80th Ed. (CRC Press, Boca Raton, FL, 1999–2000).
[37] J. Berkowitz, G.B. Ellison and D. Gutman, J. Phys. Chem. 98 (1994) 2744.
[38] G.B. Ellison, G.E. Davico, V.M. Bierbaum and C.H. DePuy, Int. J. Mass Spectrom. Ion Proc. 156 (1997) 109.
[39] J.B. Pedley and E.M. Marshall, J. Phys. Chem. Ref. Data 12 (1984) 967.
[40] O.M. Uy and J. Drowart, Trans. Faraday Soc. 65 (1969) 3221.
[41] H.-P. Loock, B. Simard, S. Wallin and C. Linton, J. Chem. Phys. 109 (1998) 8980.
[42] M. Chen, U.V. Waghmare, C.M. Friend and E. Kaxiras, J. Chem. Phys. 109 (1998) 6854.
[43] K. Hermann, M. Witko and A. Michalak, Catal. Today 50 (1999) 567.
[44] L.C. Glaeser, J.F. Brazdil, M.A. Hazle, M. Mehicic and R.K. Grasselli, J. Chem. Soc. Faraday Trans. I 81 (1985) 2903.
[45] R.K. Grasselli, J. Chem. Educ. 63 (1986) 216.
[46] H. Mizoguchi, H. Kawazoe, H. Hosona and S. Fujitsu, Solid State Commun. 104 (1997) 705.
[47] H. Mizoguchi, K. Ueda, H. Kawazoe, H. Hosono, T. Omata and S. Fujitsu, J. Mater. Chem. 7 (1997) 943.
[48] R.K. Grasselli and J.L. Callahan, J. Catal. 14 (1969) 93.
[49] R.K. Grasselli and D.D. Suresh, J. Catal. 25 (1972) 273.
[50] H.E. Swift, J.E. Bozik and J.A. Ondrey, J. Catal. 21 (1971) 212.
[51] R.K. Grasselli, Appl. Catal. 15 (1985) 127.
[52] J.D. Burrington, C.T. Kartisek and R.K. Grasselli, J. Catal. 87 (1984) 363.